Lawrence Berkeley National Laboratory
Chemical Sciences

Title
Atomically Thick Pt-Cu Nanosheets: Self-Assembled Sandwich and Nanoring-Like Structures

Authors
Saleem, Faisal
Xu, Biao
Ni, Bing
et al.

Atomically Thick Pt-Cu Nanosheets: Self-Assembled Sandwich and Nanoring-Like Structures

Faisal Saleem, Biao Xu, Bing Ni, Huiling Liu, Farhat Nosheen, Haoyi Li, and Xun Wang*

To minimize the use of precious metals such as Pt, there is an urgent need to develop nanostructures at the atomic scale. Since carbon-based one-atom-thick materials have shown attractive properties,[1–5] so it was attempted to prepare 2D atomic-layer-thick nanomaterials from transition metal chalcogenides[6] These layered 2D nanomaterials have covalent bonds within a layer but weak van der Waals interactions are the only interlayer bonding that gives them mechanical stability. But developing metal-based materials of this kind is challenging because they tend to develop into stable, closed-packed 3D structures. Recently, ultrathin rhodium and iron membranes of atomic scale thickness have been reported.[7,8] Nanosheets of other noble metals with a thickness around 10 atoms have also been reported.[9,10] In this respect, our group has recently reported Pt-Cu nanosheets with a minimum thickness of four atoms. However, at this stage they became unstable, resulting in curved nanosheets.[11] Thus, to the best of our knowledge, so far there is no report on the development of 2D noble metal-based alloy nanosheets less than four atoms thick. Hence, as a matter of fact, metallic 2D nanomaterials, even monometallic ones, of atomic thickness are still rare.

Here, we report a most unusual Pt-Cu 2D alloy material that is 1–2 atoms thick prepared by slightly modifying our previous methodology. This simple modification of the previous methodology leads to Pt-Cu nanosheets of single-atom thickness. Ascorbic acid (AA) and potassium iodide (KI) play a crucial role in the synthesis of nanosheets. As we reported previously, KI controls the thickness and size of the nanosheets, but the nanosheets become unstable and curve when they reach the thickness of four atoms because of their larger lateral sizes.[11] The main problem is to control the thickness without increasing the lateral size that makes them unstable. It is well known that the size of nanoparticles can be controlled by generating the nuclei at the beginning of the reaction using strong reducing agents. Very recently, Yu Huang's group prepared AuPd nanowheels with controllable sizes by varying the amount of AA.[12] Thus in the study reported here, we also used AA to increase the number of nuclei at the beginning of the reaction and thus to decrease the lateral size of the nanosheets. Reactions with AA yielded a separable product within 5 min, while without AA no product was obtained even after 15 min. The average sizes of the nanostructures obtained in the presence of AA,

4 nm (Figure S1 in the Supporting Information) and 12 nm with 0.02 g and 0.03 g KI, respectively, are comparatively small as compared to other studies that did not use AA, for the same amounts of KI.[11] So, AA is worth using as it differentiates the present study from previous studies. Next, we loaded Pd and Pt on the surface of nanosheets. Nanometer-sized sandwich-like structures were developed by loading Pd, while nanoring-like nanosheets were obtained upon Pt loading. It is not easy to develop core–shell nanostructures with a large-lattice-constant metal shell because it is well known that the lattice constant of the shell metal should be less than that of the core metal for the development of core–shell nanostructures,[13] but in our case, since the core of Pt-Cu has a smaller lattice constant than Pd and Pt, a high lattice mismatch is created in reverse. Moreover, an alloy core (Pt-Cu) and alloy shell (Pd-M) with superior activities for oxidation of formic acid have further made this work unique. PtCu@PdIr shows the highest specific activity (1.46 mA cm^{-2}) while PtCu@PdRh has the highest mass activity (773 mA/mg(Pt+Pd)).

Transmission electron microscopy (TEM) characterization shows the purity of the nanosheets, self-assembled sandwich structures, and nanoring-like nanosheets. The nanosheets and nanoring-like nanosheets seem to be parallel to the TEM grid while the sandwich structures are almost vertical (perpendicular). **Figure 1**a shows the average size of these nanosheets is around 12 nm. Further careful analysis shows that these nanosheets are highly flexible, in fact they have a slight curve and TEM also shows their thickness is about 0.17 nm (inset of Figure 1a). Under a strong electron beam, these atomic-thickness nanosheets rearrange themselves into hollow or small particles (Figure S2, Supporting Information), which indicates that these nanosheets are super thin.[7] Fourier transform infrared (FTIR) spectroscopy was used to verify whether ascorbic acid is adsorbed on the surface of nanosheets. FTIR spectra clearly show a difference between pure AA and final nanosheets obtained in the presence of AA. The absence of strong stretching peaks of –OH and carbon–carbon double bonds indicates that AA is not adsorbed on the nanosheets. However, a strong peak of the carbonyl group is shifted from 1672 cm^{-1} (pure poly(vinylpyrrolidone), PVP) to a lower frequency, 1640 cm^{-1}, owing to the strong interaction between the carbonyl group of PVP and metal atoms of the nanosheets.[7] This red shift is more obvious in the presence of AA than for nanosheets prepared in the absence of AA under the same conditions. This strong interaction may play an important role in the stability of these nanosheets just a single atom thick.

All sandwich structures are highly self-assembled (Figures 1c,d and 3) and this self-assembly may occur as a result of energetically and entropically favored face-to-face interactions.[14,15] Although various techniques[16–18] have been developed for self-assembled 2D nanostructures, it is hard to justify

F. Saleem, Dr. B. Xu, B. Ni, H. L. Liu, F. Nosheen,
H. Y. Li, Prof. X. Wang
Department of Chemistry
Tsinghua University
Beijing 100084, P. R. China
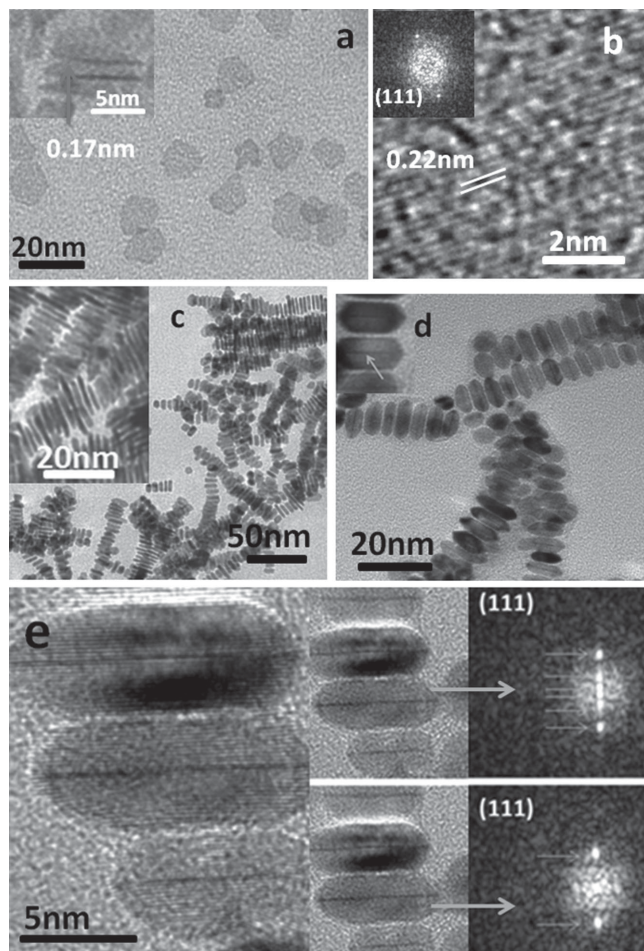E-mail: wangxun@mail.tsinghua.edu.cn

COMMUNICATION

Figure 1. a) Pt-Cu nanosheets. Inset: The nanosheets have a slight curve. b) HRTEM image showing the lattice spacing. Inset: FFT pattern. c) TEM image of PtCu@Pd1. Inset: Higher magnification image. d) PtCu@Pd2. Inset: Higher magnification image. e) HRTEM images (left) with FFT patterns (right) from the center (top) and edge (bottom).

the reason for the existence of these self-assembled sandwich structures because nanosheets and nanoring-like nanosheets are not self-assembled, even though they were all prepared under the same experimental conditions. The thickness of the sandwich structures can be varied from 1–2 nm (PtCu@Pd1) to 4–5 nm (PtCu@Pd2) by increasing the amount of Pd (Figure 1c,d) but the distance between the self-assembled particles remains around 0.6 nm. This small inter-particle distance indicates the strong interaction between self-assembled nanostructures. High-resolution TEM (HRTEM) images show that the visible lattice fringes correspond to a spacing of 0.22 nm, which matches well with the expected spacing of the (111) plane of the Pt-Cu alloy (inset in Figure 1b). Similarly, a lattice spacing of 0.23 nm also matches well with the expected spacing of the (111) plane of the PtCu@Pd2 nanosandwich (**Figures** 1e and **2**c). Differences between fast Fourier transform (FFT) patterns of sandwich structures from the center and side areas clearly show that the inner part of the sandwich structure contains Pt-Cu nanosheeets (Figure 1e and Figure S4, Supporting Information). HRTEM (**Figures** 1e and **3**c) clearly shows the contrast between core and shell: the deep black inner part represents
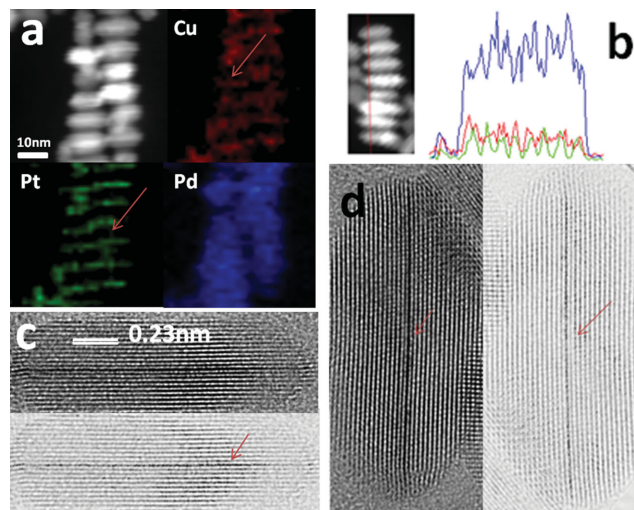

Figure 2. a) Elemental mapping. b) Line scanning profile of sandwich structures. Blue, red, and green lines represent Pd, Cu, and Pt, respectively. c,d) HRTEM images of two sandwich structures with their bright-field images. Arrows indicate the inside nanosheets.

Pt-Cu while the lighter outer part indicates the shell. After taking HRTEM images of more than 50 sandwich structures, we concluded that single-atom-thickness nanosheets containing nanosandwich structures are in the majority. Interestingly, no nanosheet with a thickness of three or more atoms was found among all these analyzed nanostructures. Elemental mapping has further shown the position and presence of a core and a shell (Figure 2a). As the thickness of the Pd shell decreases it becomes difficult to distinguish between core and shell of these sandwich structures with elemental mapping as the structures may no longer remain completely vertical on the TEM grid.

The same procedure was further extended to introduce other metals, such as Rh, Ru, and Ir, into these PtCu@Pd1 nanosandwich structures (Figure 3). Elemental mapping and line-scanning profiles have confirmed the presence of these metals (Figures S5a, S6a, and S7a, Supporting Information). The X-ray diffraction (XRD) patterns of Pt-Cu and the sandwich structures are shown in Figure S8 (Supporting Information). It is clear that peaks for Pt-Cu(111) are shifted from a high theta angle value to a low value after Pd has been loaded on the surface of the nanosheets. Energy dispersive X-ray spectroscopy (EDS) complemented with TEM has clearly shown the presence of Ir, Rh, and Ru in these structures, but their percentage of the total composition is very low compared to Pd (Figure S10, Supporting Information). This is further confirmed by inductively coupled plasma optical emission spectrometry (ICP-OES) and a line scanning profile, which indicates the presence of more Pd than other elements in these sandwich structures (Figures S5b, S6b, and S7b, Supporting Information).

Pt behaved totally differently from Pd when loaded on the surface of nanosheets. It only attaches at the edge, leading to thick-edge nanosheets (**Figure 4**), instead of forming sandwich-like structures. Here the lattice constants of Pd and Pt play an important role. Upon comparison of the lattice mismatch of (111) planes of Pd and Pt with Pt-Cu, Pd is found to be closer to Pt-Cu, so it loads on nanosheets easily, while Pt, having a much larger lattice mismatch with Pt-Cu, goes at the more energetic
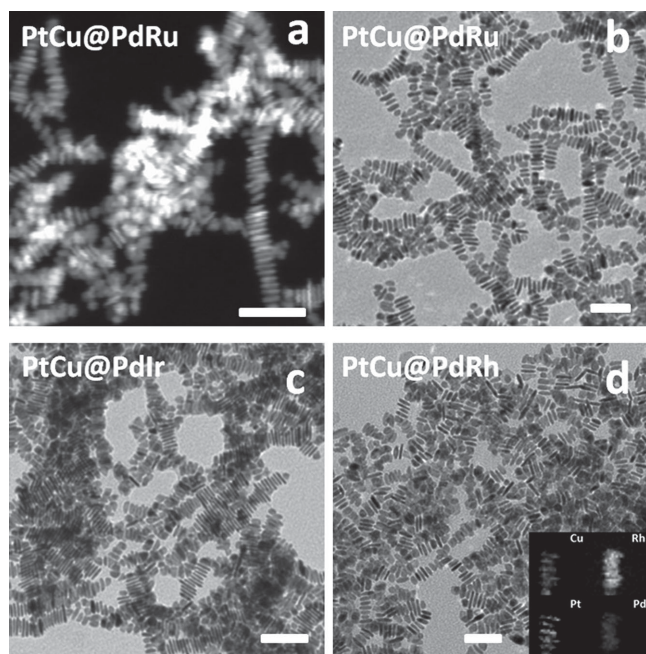
Figure 3. Self-assembled nanosandwich structures. a,b) Dark-field image (a) and TEM image (b) of PtCu@PdRu. c) TEM image of PtCu@PdIr. d) TEM image of PtCu@PdRh. Inset: Elemental mapping. Scale bars correspond to 50 nm.
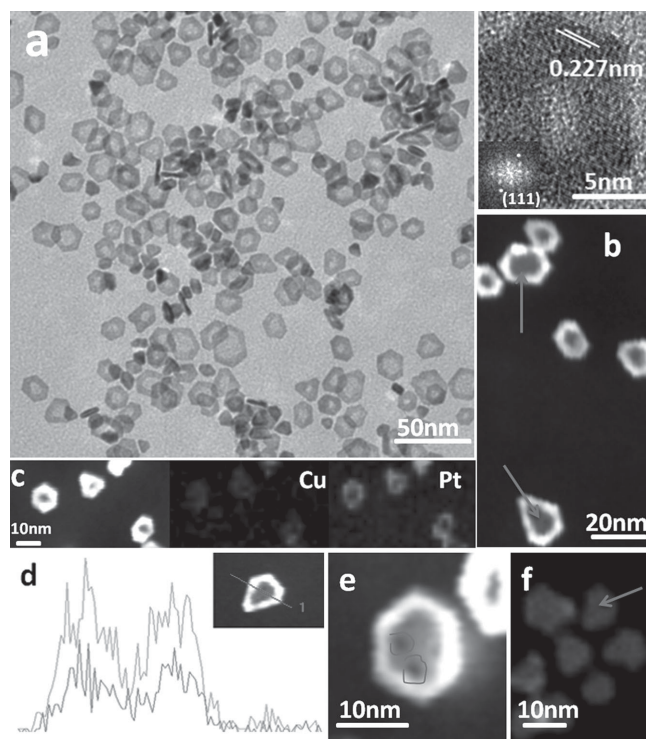

Figure 4. a) TEM image of thick-edge nanosheets. Top right: HRTEM image showing lattice spacing. Inset: FFT pattern. b) Dark field image. c) Elemental mapping. d) Line scanning profile. Red and green lines correspond to Cu and Pt, respectively. e) Dark-field image of a single particle. The red lines mark holes in it. f) Simple nanosheets.

edges of nanosheets. Dark field images of both nanosheets (Figure 4f) and nanoring-like structures (Figure 4b) clearly show that the central part is not empty, although there are some pores there (Figure 4e). A line scanning profile indicates that Pt is loaded at the peripheral surface of nanosheets and that some Cu etched out from the center during reaction (Figure 4d). The same reaction was also performed with three times the amount of Pt, but it didn't affect the morphology (Figure S11, Supporting Information). This means that only a specific amount of Pt can be loaded at the edges. XRD (Figure S8, Supporting Information) and EDS (Figure S10b, Supporting Information) also confirmed the loading of Pt. We also added Au ions, which have an even greater lattice mismatch than Pt, under the same reaction conditions, but no loading of Au was observed; nanoparticles can also be observed in the TEM image, in addition to nanosheets (Figure S12, Supporting Information). Thus the behavior of loading of Pd, Pt, and Au appears to depend totally on the lattice mismatch with the nanosheets, under the same reaction conditions, while loading of Pt at the edges may be induced by high energy in the peripheral region of these nanosheets. Cheon's group also observed the same behavior of loading and edge-selective reaction on TiS_2 nanodiscs.[19,20]

The great potential of formic acid fuel cells as an energy source in portable electronic devices has focused the interest of many researchers on the electrochemical oxidation of formic acid. It is well documented that oxidation of formic acid proceeds through two pathways, one is direct and other is an indirect (poisoning) pathway. In the direct pathway, formic acid is directly dehydrogenated and generates CO_2, while in the poisoning (indirect) pathway formic acid dehydrates and generates carbon monoxide (CO), which further oxidizes to CO_2. As this CO

(self-poisoning intermediate) liberated in the poisoning pathway deactivates the active sites of the catalyst,[21–23] so direct pathway is highly desired for the oxidation of formic acid. This process is usually found on the surface of Pd-based catalysts in formic acid fuel cells.[21,22,24] Furthermore, direct oxidation of formic acid takes place at a lower potential and also produces more energy (-48.4 kJ mol^{-1}) than the indirect pathway (-28.5 kJ mol^{-1}).[23] Researchers have used nanoparticles for direct oxidation of formic acid,[25–29] but core–shell nanostructures were found to be more effective[23,30–33] because the physical and chemical properties of the outer shell metal are totally changed by the influence of the inner core of the other metal element.[34,35] Tsang's group prepared core–shell nanostructures with different core metals but using Pd as a shell, and found that oxidation of formic acid by an outer Pd shell is electronically promoted by an inner Ag core.[23] As Pd is best for formic acid oxidation, we compared our nanosheets, nanosandwiches, and nanoring-like structures with Pd/C.[36] The new structures showed high specific and mass activities compared to Pd/C. As it is well documented that alloy nanostructures always have better electrocatalytic activities than their corresponding individual monometallic nanostructures, we developed an outer Pd-based alloy shell by introducing other metals, such as Ru, Ir, or Rh, and they showed high catalytic activity compared to a non-alloyed, pure Pd shell.

All these sandwich structures have shown direct oxidation of formic acid at low voltage. To check their stability, we subjected a PtCu@Pd2 catalyst to two trials, each of 30 cycles. In the second trial, with fresh formic acid solution, the performance of the

catalyst even increased slightly, confirming the high stability of the catalyst under these conditions (Figure S13, Supporting Information). Furthermore, we took TEM images of these structures after electrocatalysis to confirm the structure stability; there was no observable change in the structures, and so they can be maintained during oxidation (Figure S14, Supporting Information). Nanoring-like structures also show high activity for oxidation of formic acid, but in the poisoning region at high potential, above 0.7 V. They also have another peak at low voltage, near 0.4 V, but since its intensity is low, the main product is carbon monoxide instead of carbon dioxide, which can deactivate the catalyst. To demonstrate the stability of nanoring-like structures, after electrocatalysis we took TEM, HRTEM, and dark field images and also line scanning profiles. All analyses showed that even the inner part of these structures is still stable under electrocatalysis (Figure S15, Supporting Information).

Figure 5 shows only forward anodic cycles of specific and mass activities for formic acid oxidation with commercial Pd/C, Pt-Cu/C nanosheets and their sandwich structures, and thick-edge nanosheets. The specific current density (J) was normalized to the electrochemically active surface area (ECSA),

which is estimated from the hydrogen adsorption/desorption charges by using cyclic voltammetry (CV) data in 0.5 M H_2SO_4, assuming 210 μC cm^{-2}. CV measurements were performed under N_2 at room temperature, and potential was scanned from -0.2 to 0.8 V (vs. saturated calomel electrode, SCE) at a sweep rate of 50 mV s^{-1}. All newly prepared catalysts exhibited higher catalytic activity than commercial Pd/C. PtCu@PdIr has the highest catalytic activity, 1.46 mA cm^{-2}, which is almost 8.6 times that of commercial Pd/C (0.17 mA cm^{-2}). The order of decreasing overall specific activity is for these particles PtCu@PdIr > PtCu@PdRh > PtCu@PdRu > PtCu with thick edge > Pt-Cu/C > PtCu@Pd1 > PtCu@Pd2 > Pd/C.

ECSAs and mass activities of nanosheets and nanoring-like nanostructures were normalized only with Pt while for sandwich structures both Pt and Pd (Pt+Pd) were used. Similarly, PtCu@PdRh showed the highest ECSA [m^2/g(Pt+Pd)] among these sandwich structures. They can be arranged in decreasing order of ESCA as PtCu@PdRh > PtCu@Pd2 > PtCu@PdIr > PtCu@Pd1 > PtCu@PdRu.

In the case of mass activity [mA/mg(Pt+Pd)], PtCu@PdRh again showed the highest mass activity among these sandwich

(1) Pd/C, **(2)** PtCu/C, **(3)** PtCu@Pd1, **(4)** PtCu@Pd2, **(5)** PtCu@PdRu, **(6)** PtCu@PdIr, **(7)** PtCu@PdRh, **(8)** PtCu with Thick Edge
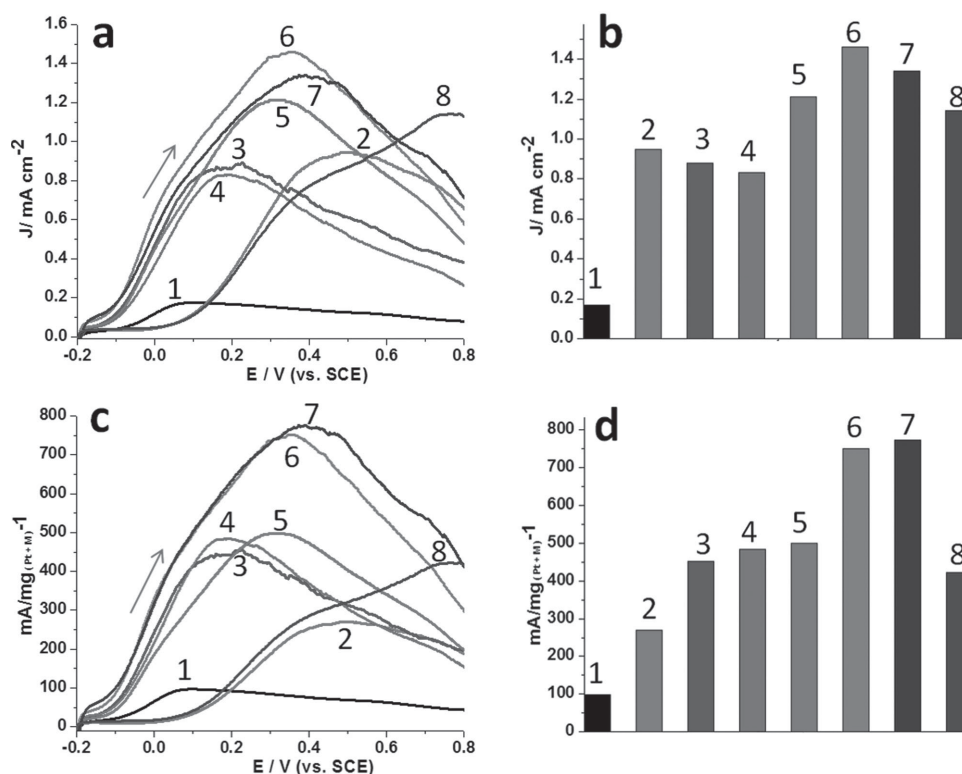

Figure 5. Comparison study between commercial Pd/C, Pt-Cu nanosheets with their sandwich and nanoring like structures for formic acid oxidation at room temperature at a scan rate of 50 mV s^{-1} in N_2 purged solution. a) Specific (mA cm^{-2}) activities. b) Maximum specific activities. c) Mass activities. d) Maximum mass activities. Specific and mass activities are given as kinetic current densities (J) normalized with respect to the ECSA and loading amount of metal. Current densities were normalized with respect to the geometric area of a working electrode (0.07). The formic acid oxidation was recorded in 0.5 M H_2SO_4 + 0.1 M HCOOH solution at the same scan rate. All samples have the same shading in (a–d) and the arrow's direction shows only the forward anodic cycles.

nanostructures, about 7.8 times that of commercial Pd/C. Their order of mass activity (Figure 5c) is PtCu@PdRh > PtCu@PdIr > PtCu@PdRu > PtCu@Pd2 > PtCu@Pd1. Similarly, nanosheets and nanoring-like structures also have high activities. Details are given in Table 1 in the Supporting Information.

In summary, we have efficiently investigated a chemical method for controlled synthesis of atomically thick freestanding unique Pt-Cu nanosheets and proved that alloy nanosheets of one atom thickness can be obtained. Using these nanosheets as seeds, we developed highly effective and novel sandwich and nanoring-like structures. Different metals of different lattice constants compared to Pt-Cu nanosheets were added to them to prove that these nanosheets have two energy regions and loading depends on lattice mismatch. Further, these nanosandwich structures displayed direct oxidation for formic acid with high activities. These as-synthesized nanostructures can further be used efficiently in ongoing studies for the development of dual-alloy-based core–shell nanostructures with improved electrocatalytic activity.

Experimental Section

Reagents: A hydrothermal procedure was adopted that used commercially available reagents: $Cu(acac)_2$ (Alfa Aesar), $Pt(acac)_2$ (Alfa Aesar), $RuCl_3 \cdot xH_2O$ (Alfa Aesar), $PdCl_2$ (Alfa Aesar), $RhCl_3 \cdot xH_2O$ (Alfa Aesar), $IrCl_3 \cdot xH_2O$ (Alfa Aesar), poly(vinylpyrrolidone) (PVP; Mw 8000, Alfa Aesar), KI (Sinopharm Chemical Reagent Co.), tris(hydroxymethyl)aminomethane (Sinopharm Chemical Reagent Co.), HCHO solution (37 wt%; Sinopharm Chemical Reagent Co.), formamide, and acetone (Sinopharm Chemical Reagent Co.).

Synthesis of Atomically tTick Pt-Cu Nanosheets and Their Sandwich and Nanoring-Like Structures: A solution of PVP (200 mg) and tris(hydroxymethyl)aminomethane (50 mg) in HCHO (2 mL) was heated at 200 °C in a 12 mL poly(tetrafluoroethylene) (Teflon)-lined stainless steel autoclave for 3 h. The resulting gel-like material was washed and dried after centrifugation at 10000 rpm in acetone.[11] A homogeneous solution of 0.01 mmol $Cu(acac)_2$, 0.01 mmol $Pt(acac)_2$, 0.03 g ascorbic acid, and 0.03 g KI was also prepared in 2mL formamide in the same autoclave at 130 °C for 3 h. Nanosheets were obtained after the addition of acetone followed by centrifugation. The previously used amount of gel, 200 mg PVP and 50 mg tris(hydroxymethyl)aminomethane in 2 mL HCHO at 200 °C, was added to these nanosheets along with 0.06 g KI and 2 mL formamide. The mixture was autoclaved for 3 h at 130 °C after a specific amount of specific precursor had been added, depending on the desired shell type, as listed here. PtCu@Pd1: 0.01 mmol $PdCl_2$; PtCu@PdRu: 0.01 mmol $PdCl_2$ and 0.01 mmol $RuCl_3 \cdot xH_2O$; PtCu@PdIr: 0.01 mmol $PdCl_2$ and 0.01 mmol $IrCl_3 \cdot xH_2O$; PtCu@PdRh: 0.01 mmol $PdCl_2$ and 0.01 mmol $RhCl_3 \cdot xH_2O$; PtCu@Pd2: 0.035 mmol $PdCl_2$; nanoring-like structure: 0.01 mmol $Pt(acac)_2$. Washing was finally done by using acetone and ethanol.

Electrochemical Tests: Electrochemical tests were performed using a CHI650D electrochemical analyzer (CHI Instruments, TX, USA). A conventional three-electrode cell, containing a Pt wire as the counter electrode, a SCE as the reference electrode, and a glassy carbon (GC) electrode (3 mm in diameter) as the working electrode, was used. Electrode potentials are quoted versus the SCE. The GC electrode was polished with Al_2O_3 paste, washed with ethanol and deionized water, and dried before use. A weighed amount of carbon black was added to Pt-Cu nanosheets dispersed in water and sonicated for 1 h. Solution was loaded gradually on the GC electrode by using a micro syringe with the same loading of 8 µL. The concentration of all catalysts in the aqueous solution was determined by ICP-OES. After the ink had dried, Nafion polymer in alcohol solution (Alfa Aesar; 0.5 wt%, 1.5 µL) was added and again dried in air for some time. Electrolyte

was freshly made by bubbling N_2 in a solution of 0.5 M H_2SO_4 and 0.1 M HCOOH . CV measurements were performed under N_2 at room temperature, and potential was scanned from –0.2 to 0.8 V (vs. SCE) at a sweep rate of 50 mV s^{-1}. The ECSA of each sample was estimated by CV measurements carried out in fresh nitrogen-saturated 0.5 M H_2SO_4 solution, and the potential was scanned from –0.24 to 0.8V (vs. SCE) at a sweep rate of 50 mV s^{-1}.

Supporting Information

Supporting Information is available from the Wiley Online Library or from the author.

Acknowledgements

[1] M. Chhowalla, H. S. Shin, G. Eda, L.-J. Li, K. P. Loh, H. Zhang, *Nat. Chem.* **2013**, *5*, 263.

[2] A. K. Geim, *Science* **2009**, *324*, 1530.

[3] K. S. Novoselov, A. K. Geim, S. V. Morozov, D. Jiang, Y. Zhang, S. V. Dubonos, I. V. Grigorieva, A. A. Firsov, *Science* **2004**, *306*, 666.

[4] Y. Zhang, Y.-W. Tan, H. L. Stormer, P. Kim, *Nature* **2005**, *438*, 201.

[5] X. Huang, Z. Yin, S. Wu, X. Qi, Q. He, Q. Zhang, Q. Yan, F. Boey, H. Zhang, *Small* **2011**, *7*, 1876.

[6] Y.-H. Lee, X.-Q. Zhang, W. Zhang, M.-T. Chang, C.-T. Lin, K.-D. Chang, Y.-C. Yu, J. T.-W. Wang, C.-S. Chang, L.-J. Li, T.-W. Lin, *Adv. Mater.* **2012**, *24*, 2320.

[7] H. Duan, N. Yan, R. Yu, C.-R. Chang, G. Zhou, H.-S. Hu, H. Rong, Z. Niu, J. Mao, H. Asakura, T. Tanaka, P.-J. Dyson, J. Li, Y. Li, *Nat. Commun.* **2014**, *5*, 3093.

[8] J. Zhao, Q. Deng, A. Bachmatiuk, G. Sandeep, A. Popov, J. Eckert, M. H. Rümmeli, *Science* **2014**, *343*, 1228.

[9] X. Huang, S. Tang, X. Mu, Y. Dai, G. Chen, Z. Zhou, F. Ruan, Z. Yang, N. Zheng, *Nat. Nanotechnol.* **2011**, *6*, 28.

[10] K. Jang, H. J. Kim, S. U. Son, *Chem. Mater.* **2010**, *22*, 1273.

[11] F. Saleem, Z. Zhang, B. Xu, X. Xu, P. He, X. Wang, *J. Am. Chem. Soc.* **2013**, *135*, 18304.

[12] X. Huang, Y. Li, Y. Chen, H. Zhou, X. Duan, Y. Huang, *Angew. Chem. Int. Ed.* **2013**, *52*, 6063.

[13] F.-R. Fan, D.-Y. Liu, Y.-F. Wu, S. Duan, Z.-X. Xie, Z.-Y. Jiang, Z.-Q. Tian, *J. Am. Chem. Soc.* **2008**, *130*, 6949.

[14] C. Hou, J. Zhu, C. Liu, X. Wang, Q. Kuang, L. Zheng, *CrystEngComm* **2013**, *15*, 6127.

[15] X. Ye, J. Chen, M. Engel, J. A. Millan, W. Li, L. Qi, G. Xing, J. E. Collins, C. R. Kagan, J. Li, S. C. Glotzer, C. B. Murray, *Nat. Chem.* **2013**, *5*, 466.

[16] Y. Bae, N. H. Kim, M. Kim, K. Y. Lee, S. W. Han, *J. Am. Chem. Soc.* **2008**, *130*, 5432.

[17] V. F. Puntes, D. Zanchet, C. K. Erdonmez, A. P. Alivisatos, *J. Am. Chem. Soc.* **2002**, *124*, 12874.

[18] C. Hu, K. Lin, X. Wang, S. Liu, J. Yi, Y. Tian, B. Wu, G. Chen, H. Yang, Y. Dai, H. Li, N. Zheng, *J. Am. Chem. Soc.* **2014**, *136*, 12856.

[19] S. Jeong, J. H. Han, J.-t. Jang, J.-w. Seo, J.-G. Kim, J. Cheon, *J. Am. Chem. Soc.* **2011**, *133*, 14500.

[20] J. H. Han, S. Lee, D. Yoo, J.-H. Lee, S. Jeong, J.-G. Kim, J. Cheon, *J. Am. Chem. Soc.* **2013**, *135*, 3736.

[21] F. J. Vidal-Iglesias, J. Solla-Gullón, E. Herrero, A. Aldaz, J. M. Feliu, *Angew. Chem. Int. Ed.* **2010**, *49*, 6998.

[22] E. Antolini, *Energy Environ. Sci.* **2009**, *2*, 915.

[23] K. Tedsree, T. Li, S. Jones, C. W. A. Chan, K. M. K. Yu, P. A. J. Bagot, E. A. Marquis, G. D. W. Smith, S. C. E. Tsang, *Nat. Nanotechnol.* **2011**, *6*, 302.

[24] J. W. Hong, D. Kim, Y. W. Lee, M. Kim, S. W. Kang, S. W. Han, *Angew. Chem. Int. Ed.* **2011**, *50*, 8876.

[25] J. Wang, D. F. Thomas, A. Chen, *Chem. Commun.* **2008**, 5010.

[26] S. Yang, C. Shen, Y. Tian, X. Zhang, H.-J. Gao, *Nanoscale* **2014**, *6*, 13154.

[27] J. Zhang, H. Chen, H. Li, J. Di, M. Chen, F. Geng, Z. Zhao, Q. Li, *Chem. Mater.* **2014**, *26*, 2789.

[28] J. Chang, L. Feng, C. Liu, W. Xing, X. Hu, *Angew. Chem. Int. Ed.* **2014**, *53*, 122.

[29] X. Ji, K. T. Lee, R. Holden, L. Zhang, J. Zhang, G. A. Botton, M. Couillard, L. F. Nazar, *Nat. Chem.* **2010**, *2*, 286.

[30] Y. Kang, L. Qi, M. Li, R. E. Diaz, D. Su, R. R. Adzic, E. Stach, J. Li, C. B. Murray, *ACS Nano* **2012**, *6*, 2818.

[31] Y. Huang, X. Zhou, M. Yin, C. Liu, W. Xing, *Chem. Mater.* **2010**, *22*, 5122.

[32] M. Rezaei, S. H. Tabaian, D. F. J. Haghshenas, *Mater. Chem. A* **2014**, *2*, 4588.

[33] P.-P. Fang, S. Duan, X.-D. Lin, J. R. Anema, J.-F. Li, O. Buriez, Y. Ding, F.-R. Fan, D.-Y. Wu, B. Ren, Z. L. Wang, C. Amatore, Z.-Q. Tian, *Chem. Sci.* **2011**, *2*, 531.

[34] F. Tao, M. E. Grass, Y. Zhang, D. R. Butcher, J. R. Renzas, Z. Liu, J. Y. Chung, B. S. Mun, M. Salmeron, G. A. Somorjai, *Science* **2008**, *322*, 932.

[35] H. Kobayashi, M. Yamauchi, H. Kitagawa, Y. Kubota, K. Kato, M. Takata, *J. Am. Chem. Soc.* **2008**, *130*, 1818.

[36] R. Larsen, S. Ha, J. Zakzeski, R. I. Masel, *J. Power Sources* **2006**, *157*, 78.